Journal of Applied Polymer Science

Mechanical, Water Absorption, and Morphology of Recycled Polymer Blend Rice Husk Flour Biocomposites

Ruey Shan Chen, Mohd Hafizuddin Ab Ghani, Mohd Nazry Salleh, Sahrim Ahmad, Mou'ad A. Tarawneh

Material Science Programme, School of Applied Physics, Faculty of Science and Technology, The National University of Malaysia, 43600 Bangi, Malaysia

Correspondence to: R. S. Chen (E-mail: rueyshanchen@hotmail.com)

ABSTRACT: Rice husk flour (RHF) biocomposites based on uncompatibilized and compatibilized recycled high density polyethylene/recycled polyethylene terephthalate (rHDPE/rPET) with ethylene-glycidyl methacrylate (E-GMA) copolymer were prepared through a two-step extrusion and hot pressing with fiber loadings of 40, 60, and 80 wt %. Results showed that tensile and flexural properties increased. However, the elongation to break and impact strength decreased as the RHF loading increased. Compatibilizing polymer blend matrices can further enhance the mechanical properties. Water absorption (WA) test were examined in distilled and seawater. It is interesting to note that for composites made from uncompatibilized matrix, the calculated D and K_{SR} were lower in seawater, but for the compatibilized matrix composites, the D and K_{SR} obtained were generally lower in distilled water. However, compatibilization of rHDPE/rPET has been markedly reduced the WA and thickness swelling. Scanning electron microscope analysis of the compatibilized matrix composites confirmed the improved interfacial bonding of matrix–matrix and filler–matrix phases. © 2014 Wiley Periodicals, Inc. J. Appl. Polym. Sci. **2015**, *132*, 41494.

KEYWORDS: composites; extrusion; fibers; mechanical properties; thermoplastics

Received 20 May 2014; accepted 3 September 2014

DOI: 10.1002/app.41494

INTRODUCTION

Waste plastic industrial and agricultural materials are currently becoming of interest worldwide in the field of composite materials, as a result of the increasing demand for environmentally friendly raw materials. Rice husk (RH) is an agro-waste that is generated in large quantities during the rice-milling process in rice-producing countries.[1] In the paddy plants of Malaysia, with a land area of approximately 680,000 hectares, a total of 840,000 tons of RH is produced every year.[2] RH is a cellulose-based fibrous material with a wide range of aspect ratios.[3] The incorporation of RH into polymer matrices provides advantageous characteristics, such as biodegradability, lightweight, toughness, and resistance to weathering, and also makes the final products more economically competitive.[4,5] Compared with wood-based composites, the RH-filled composites have higher resistance to termite and biological attack, and also better dimensional stability upon exposure to moisture. Thus, these composites are increasingly being used in building construction, such as frames for windows and doors, slidings, decks, interior panels, and in the automotive industry for interior parts like door panels and trims.[1]

In the production of natural fiber plastic composites (NFPCs), both thermoplastic and thermoset plastic can be used, in either virgin or recycled form. However, the waste plastics offer a promising source of raw material for the composites because of the huge amount generated every day and the lower cost than virgin plastics.[6] Traditionally, the polymer matrix used in NFPCs is only made from a single type of plastic.[6–10] However, the studies of NFPCs based on polymer blends (PB) are very limited.[11,12] As known, high density polyethylene (HDPE) and polyethylene terepthalate (PET) are widely employed in the packaging industry and they constitute the major component of plastic waste that contributes to municipal solid waste (MSW).[13,14] Lei and Wu[11] used recycled HDPE/PET blends compatibilized with ethylene-glycidyl methacrylate copolymer (E-GMA) as the matrices for WPCs.

Moisture absorption of natural fibers is becoming a critical concern, especially for their potential outdoor use in building application.[6,9] Water absorption (WA) is an important property that determines the durability and performance of NFPCs.[9] As discussed by Tajvidi et al.,[9] WA in NFPCs is dependent upon the formulation of resultant composites and processing features

Table I. Biocomposites Formulations

Composite sample code	PB type	Polymer content (wt %)	RHF (wt %)	MAPE (phr)
UPB	Uncompatibilized	100	0	0
UPB60RHF40	Uncompatibilized	60	40	3
UPB40RHF60	Uncompatibilized	40	60	3
UPB20RHF80	Uncompatibilized	20	80	3
CPB	Compatibilized	100	0	0
CPB60RHF40	Compatibilized	60	40	3
CPB40RHF60	Compatibilized	40	60	3
CPB20RHF80	Compatibilized	20	80	3

such as processing temperature, rotating screw speed, etc., but not limited to the types of natural fiber or plastic, processing system, size, and dispersion of fiber as well as quality of interfacial. In order to improve the water resistance of NFPCs, coupling agents such as maleic anhydride polypropylene (MAPP) and maleic anhydride polyethylene (MAPE), compatibilizers, or other surface treatment of fibers such as silane.[10,15–17] As reported in previous studies, WA test has been subjected in distilled water,[6,18–20] tap water,[21] seawater,[20,22] and acidic[20,22] water to explore other possible applications of NFPCs in various environment conditions.

In this present work, we focused on WA and thickness swelling (TS) behavior of rice husk flour (RHF)/recycled PB (with and without compatibilization of E-GMA) biocomposites under distilled and seawater immersion. The equilibrium WA (M_m), diffusion coefficient (D), equilibrium thickness swelling (TS_∞) and swelling rate parameter (K_{SR}) of the composites were determined. The comparison between the experimental data and the prediction from model are reported.

EXPERIMENTAL

Raw Materials

In this study, the polymer blend (PB) matrix used was recycled high-density polyethylene (rHDPE) and recycled polyethylene terephthalate (rPET). The rHDPE has a density of 923 kg/m^3 and melt flow index of 0.72 g/10 min at 190°C, respectively. Meanwhile, rPET has a glass transition temperature of 74.1°C, cold crystallization peak temperature of 119.9°C, and melting peak temperature of 252.5°C. E-GMA, Lotader AX8840 was used to compatibilize the immiscible PBs. It has a melt flow index of 5 g/10 min (190°C, 2.16 kg) and a glycidyl methacrylate content of 8%. The agro-filler used in the experiment was 100-mesh particle size of RHF. MAPE with a melting peak temperature of 135.2°C was utilized as coupling agent. All the raw materials were obtained from a local factory namely BioComposites Extrusion Sdn. Bhd.

Preparation of Recycled HDPE/PET Blend

The rHDPE and rPET were melt-blended using a laboratory scale co-rotating twin screw extruder (Thermo Prism TSE 16PC, $D = 16$ mm, $L/D = 24$). The screw rotating speed was fixed 30 rpm. The four barrel temperatures from the feeding to die zones were set as 250°C, 270°C, 240°C and 190°C, respectively. For the uncompatibilized polymer blend (UPB), the weight ratio of rHDPE/rPET was fixed at 75/25 (wt/wt). Meanwhile, 5 phr of E-GMA was added in the compatibilized polymer blend (CPB) with the same ratio of both plastics.

Preparation of RHF Reinforced Biocomposites

The pre-extruded PB pellets were compounded with RHF and 3 phr of MAPE at temperatures profiles 170°C, 215°C, 210°C and 195°C with the same screw speed as extrusion of recycled PB. Before extrusion, RHF was dried in an oven at 90°C for 24 h in order to get rid of the moisture trapped inside RHF. After extrusion, the compression molding was carried out at 200°C under a pressure of 1000 psi using a hot/cold press machine (LP50, LABTECH Engineering Company Ltd). The preheating, venting, full pressing, and cold pressing times were set at 3, 2, 5, and 5 minutes, respectively. In this study, the experimental variables studied were PB types (UPB and CPB) and RHF content (40, 60, and 80 wt %). Table I presents the formulations of the RHF reinforced biocomposites.

Determination of Mechanical Properties

Compression-molded specimens were cut in accordance with ASTM standard D 638-03 (type I), D 790-03and D 256-05 for tensile, flexural properties, and impact strength, respectively. A universal testing machine (model Testometric M350-10CT) was used for both tensile and flexural testing, at a speed of 5 mm/min. The notched Izod impact testing was conducted using the Ray-Ran Universal Pendulum Impact System, with a velocity of 3.46 ms^{-1}, load weight of 0.452 kg, and a calibration energy of 2.765 J. All the reported results of the mechanical tests are the average of five replicates for each formulation.

WA and TS Test

WA and TS tests were performed according to the ASTM D 570-98 method. The specimens (dimension: 76.2 mm × 25.4 mm × 3.2 mm) were dried in an oven at 100°C for 24 h. The weight of the oven-dried specimens was measured using an analytical balance with a precision of 0.001 g; the dimensions (thickness, width, and length) at three different locations were measured using a digimatic calliper with a precision of 0.01 mm. Then the samples were immersed in distilled water and seawater at room temperature. The weight and dimensional changes were measured and recorded by periodic removal of the specimens from the water. The process was continued until the equilibrium or saturation point, at which time the average

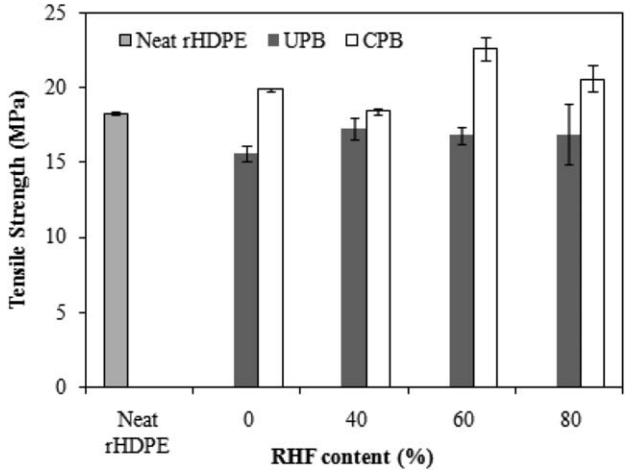

Figure 1. Tensile strength of uncompatibilized and compatibilized PB-based composites at different RHF loadings.

value of several consecutive weighings showed no appreciable additional absorption. The percentages of WA and orthotropic swelling were calculated using eq. (1):

$$\mathrm{WA}(\%) = \frac{W_t - W_0}{W_0} \times 100 \quad (1)$$

$$S(\%) = \frac{D_t - D_0}{D_0} \times 100 \quad (2)$$

where W_0 and W_t denote the oven-dry weight (the initial weight) and weight after water exposure at time t, respectively, whereas D_0 and D_t denote the oven-dry dimension and dimension after water exposure at time t, respectively.

Scanning Electron Microscopy (SEM)

The morphology of the fracture surface of each broken sample from impact testing was analyzed using SEM (Hitachi). The samples were sputter-coated with gold before examination of SEM at 1000 ×.

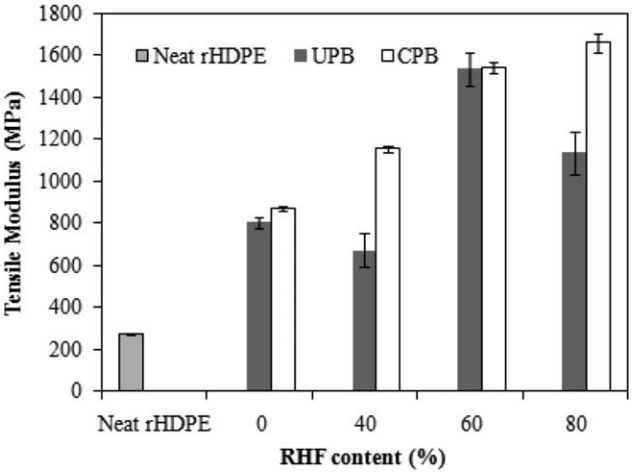

Figure 2. Tensile modulus of uncompatibilized and compatibilized PB-based composites at different RHF loadings.

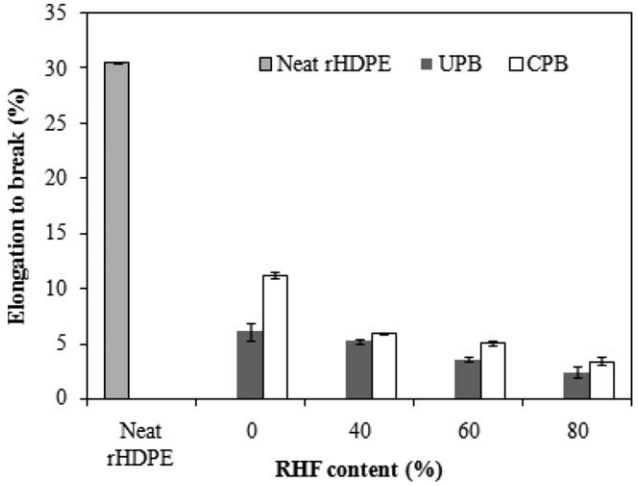

Figure 3. Elongation to break of uncompatibilized and compatibilized PB-based composites at different RHF loadings.

RESULTS AND DISCUSSION

Mechanical Properties

Tensile Properties. The effects of the type of PB matrix types and RHF loadings on the tensile strength, modulus, and elongation at break of composites are shown in Figures 1, 2, and 3, respectively. In general, the compatibilization of incompatible rHDPE and rPET by E-GMA tends to improve the tensile properties of CPB-based composites with and without RHF filler loadings. This was supported by Lei and Wu who conducted experiments on a microfibrillar blend of HDPE/PET and their WPCs.[11] The E-GMA copolymer plays an important role as compatibilizer in improving the compatibility and adhesion between rHDPE and rPET.[11,23] Therefore, the CPB blend and composites had a higher tensile strength and modulus than that of the UPB ones.

The tensile strength of the composite specimen can be influenced by the type of filler and thermoplastic matrix, any additives used such as compatibilizer or coupling agent, and the processing method of the specimen.[24] From Figure 1, the tensile strength of uncompatibilized blend and their composites filled with RHF was lower than that of neat rHDPE (18.31 MPa), by about 5.8%–14.8%. However, the introduction of 5 phr E-GMA into rHDPE/rPET blend matrices has been enhanced the tensile strength compared with the neat rHDPE and composites based on the uncompatibilized ones, which showed the recovery of tensile strength by an improvement in blend compatibility. The incorporation of RHF fiber and its content gives rise to a higher tensile strength but not significant for UPB-based biocomposites. The highest tensile strength of UPB composites was achieved for 40 wt % RHF, which increased 10.5% compared with neat UPB. This indicates the ability of fibers to transfer load effectively to one another at low fiber content. However, further increasing the RHF content up to 60–80 wt %, the tensile strength decreased very slightly (~2%) but still higher than the neat UPB. This could suggest that the insufficient wetting of fiber by the immiscible PB matrix at higher fiber loading which leads to the weak interfacial bonding between the fiber and matrix.[25,26] While, a small change but indefinite trend is found

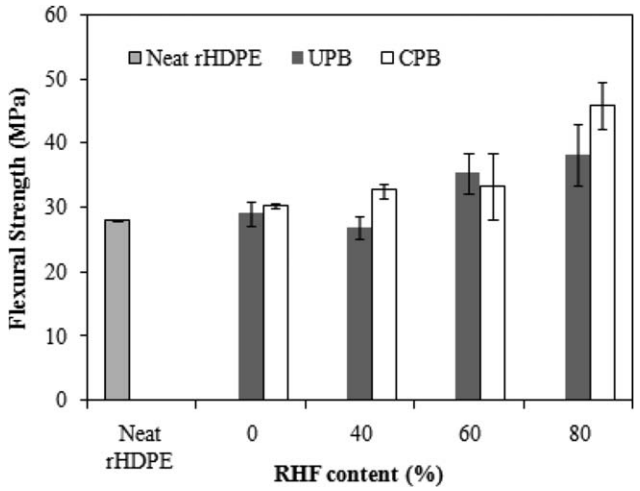

Figure 4. Flexural strength of uncompatibilized and compatibilized PB-based composites at different RHF loadings.

for the CPB-based biocomposites. Interestingly, both an increase[27] and decrease[1,28] in the tensile strength have been reported in previous work with increasing fiber content, while one researcher reported the mixed results.[19]

According to Yao et al.,[29] the tensile modulus is less sensitive to interfacial interaction compared with the tensile strength. Therefore, the increasing trend of tensile modulus that appeared in CPB-based composites (Figure 2) is associated with the stiffness gain caused by the RHF which is its intrinsic characteristic, as compared with that of neat rHDPE. This is a well-known logical trend for the composite containing low stiffness polymer matrix and high stiffness filler.[30] However, in the case of UPB-based composites, there is no specific trend associated with an increase in the RHF fiber content. It is believe that the poor interaction of the RHF–UPB matrix interface due to the incompatibility of rHDPE and rPET in UPB matrices has been taken into account for the tensile modulus. Hence, it failed to show a similar trend to that of the CPB system.

In Figure 3, the immediate steep in elongation to break with the addition of rPET into rHDPE is evident. This was due to the PET has a low elongation to break which increases the stiffness of HDPE.[31,32] As the amount of RHF fillers increased from 40 to 80 wt %, the elongation to break of composite decreased. This is ascribed to the brittle nature imparted by the RHF in the composite, indicating a decrease in the ductility of polymer matrix.[11,19] However, it is obvious that the compatibilizing rHDPE/rPET with E-GMA has been improved the elongation of the blend and their composites filled with RHF. This showed the recovery of elongation to break by 14%–85%, due to better adhesion between HDPE and PET phases.[22] The enhanced compatibility of HDPE and PET plays a significant role in improving the elongation of PB matrices as well as their composites.[11]

Flexural Properties

Figures 4 and 5 present the flexural strength and modulus of the PB-based biocomposites at different RHF loadings, respectively. The results clearly show that the presence of RHF improves the flexural properties of the biocomposites. As can be seen, a small increase in the flexural strength with filler content causes a relatively large increase in the flexural modulus of almost all the composites. According to Nourbakhsh et al.,[19] the flexural strength of fiber reinforced composites is influenced by the properties of the constituents, interfacial interaction between the fibers and the matrix, as well as the homogeneity of the whole composite. Meanwhile, in comparison to the flexural strength, the flexural modulus is typically more dependent upon the fillers, support span, environmental condition, and other factors.[33]

From Figure 4, all the CPB-based composites except for composites containing 60 wt % RHF had slightly higher flexural strength compared with the composites fabricated with the UPB matrices. It can be proven that the compatibilization of immiscible blend matrices tends to improve the mechanical characteristics of the natural fiber-based biocomposites, which was attributed to the improved adhesion between fiber and PB matrices. The addition of RHF in the blend not significantly increased the flexural strength of neat rHDPE. Meanwhile, the incorporation of RHF resulted in a remarkable increment in flexural modulus of neat rHDPE and rHDPE/rPET blend, which exhibited the similar trend as in tensile modulus. In Figure 5, the addition of E-GMA into the PB matrices as the compatibilizer for two individual polymer components decreased the overall flexural modulus of CPB-based composites. This phenomenon may be due to the introduction of the relatively compliant compatibilizer, E-GMA, which is mainly located at the rHDPE–rPET interface and which initially produces the plastic deformation.[34] Consequently, the decreased flexural modulus of the CPB matrices, compared with the UPB matrices, also causes a decrease the overall flexural modulus of their composites. However, with a lower matrix content, that is, 20 wt %, this factor can be neglected.

Impact Strength

Figure 6 shows the impact strength of the UPB- and CPB-based biocomposites at different RHF loadings. In the absence of RHF fillers, the compatibilizing role of E-GMA provides the efficient toughening, and, hence, significantly increased the impact

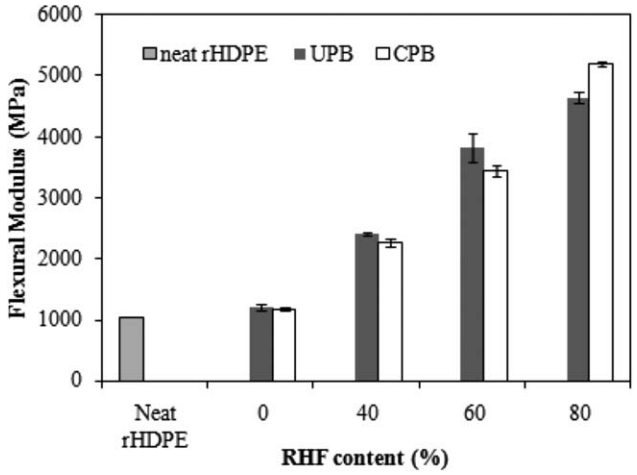

Figure 5. Flexural modulus of uncompatibilized and compatibilized PB-based composites at different RHF loadings.

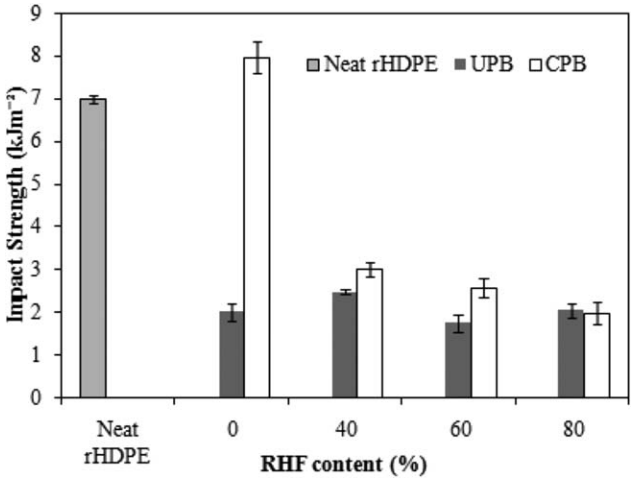

Figure 6. Impact strength of uncompatibilized and compatibilized PB-based composites at different RHF loadings.

strength of the CPB. The compatibilization of PB showed the recovery of impact strength from 2 to about 8 kJm^{-2}, which is 14% higher than that of neat rHDPE. This was attributed to the better adhesion between the rHDPE and rPET phases.[23] However, this great improvement decreased when RHF was added into the matrices, because RHF is a lignocellulosic fiber, which is a kind of stiff organic filler.[19] Note that no trend was observed for the UPB-based composites. For CPB-based composites, the impact strength slightly decreased as the filler content increased. At high filler loadings, there were many filler-filler contacts caused by the agglomeration of filler particles in the composites, which were more sensitive to crack than the filler–matrix interface. This indicates that the cracks propagated easily in the composite, and resulted in the decrease of impact strength.[35] It was also found that the addition of E-GMA in CPB matrices did not cause an improvement in the impact strength of the 80 wt % RHF reinforced composite, as revealed by the similar impact results of both the UPB and CPB-based composites. This was probably due to the higher degree of stiffness and brittleness introduced by the addition of high RHF fibers loading into the limited content of PB matrices.[36]

WA Study

Kinetics and Mechanisms of WA. In natural fiber/polymer composites, moisture/water diffusion can be governed by three possible mechanisms. First is the diffusion of water molecules via the micro-gaps between the polymer chains. Second is the capillary transportation of water molecules into the gaps and flaws at the fiber–matrix interfaces due to the poor wettability and impregnation. The third mechanism involves the transportation of water molecules by microcracks formed in the matrix during the compounding process, arising from the swelling of fibers.[20,37,38]

Prior to performing modeling of WA behavior, an analysis of the diffusion mechanism was performed in accordance with Fick's theory. This included: Case I, the Fickian diffusion where the diffusion rate is slower than that of polymer segment mobility; Case II, the relaxation controlled where the mobility of the penetrant is much greater than the other relaxation process; Case III, non-Fickian or anomalous where both the penetrant and polymer segmental mobility are comparable (intermediate diffusion behavior between Case I and II).[39] These three diffusion behaviors can be differentiated theoretically by the shape of the sorption curve plotted with experimental data represented by the Fick's equation:[12]

$$\log\left(\frac{M_t}{M_m}\right) = \log(k) + n\log(t) \tag{3}$$

where M_t and M_m are the WA at time t and maximum WA at the equilibrium state (saturation point), respectively. The constants of k and n are the diffusion kinetic parameters, and are determined from the slope and intercept of the log plot of M_t/M_m versus t which can be drawn from the experimental data, respectively. The value of coefficient n describes the different diffusion behavior as: Case I ($n = 0.5$), Case II ($n \geq 1$), and Case III ($0.5 < n < 1$).[40] Table II summarizes the diffusion kinetic parameters of RHF-filled biocomposites. It can be confirmed that all of the biocomposite formulations exhibited Fickian diffusion behavior in both solutions as the value of n is close to 0.5. A higher value of k indicates that the composite reaches the saturation point of WA in a shorter period of time. The k value was found to increase with the increasing RHF content in the composites irrespective of the PB matrix types and immersion solution. The main reason could be the increasing hydrophilicity of the resultant biocomposites due to the increased hydroxyl and carbonyl groups as the RHF content increased. Therefore, the time required to attain the saturation point of WA was longer for composites with higher RHF content. This result has been reported by Adhikary et al. concerning wood plastic composites.[10]

Water Diffusivity. The diffusion coefficient D is one of the crucial parameters of Fick's model which represents the ability of water molecules to penetrate inside the composites.[39] It can be computed using eq. (4), in the case where the values of M_t is less than 60% of the equilibrium value M_m:[41]

$$D = \pi\left[\frac{\theta h}{4M_m}\right]^2 \tag{4}$$

where D is the water diffusion coefficient; θ is the slope of the linear part of M_t against $\sqrt{t}$ curve; h is the thickness (height) of the composite sheet.[42] Once the D is known, the thermodynamic solubility (S) and permeability (P) parameters of the composites can be ascertained. The solubility is associated with

Table II. Diffusion Kinetic Parameters of RHF Filled Biocomposites

	n		k (h^{-n})	
Composite sample code	Distilled	Sea	Distilled	Sea
UPB60RHF40	0.493	0.574	0.019	0.011
UPB40RHF60	0.522	0.496	0.022	0.018
UPB20RHF80	0.489	0.424	0.800	0.095
CPB60RHF40	0.517	0.529	0.018	0.016
CPB40RHF60	0.473	0.510	0.018	0.020
CPB20RHF80	0.499	0.528	0.028	0.038

Table III. Equilibrium Water Absorption (M_m), Diffusion Coefficient (D), Solubility Parameter (S) and Permeability (P) of RHF/Recycled PB Composites in Different Immersion Environments

	M_m (%)		$D \times 10^{-13}$ (m^2 s^{-1})		S		$P \times 10^{-13}$ (m^2 s^{-1})	
Composite sample code	Distilled	Sea	Distilled	Sea	Distilled	Sea	Distilled	Sea
UPB60RHF40	6.331	5.772	1.668	1.683	0.063	0.051	0.106	0.086
UPB40RHF60	13.729	11.028	3.467	2.221	0.137	0.109	0.476	0.242
UPB20RHF80	18.974	22.936	42.540	23.692	0.190	0.229	8.072	5.433
CPB60RHF40	6.179	6.522	2.015	1.805	0.062	0.062	0.125	0.112
CPB40RHF60	9.961	11.821	1.629	2.877	0.097	0.118	0.158	0.340
CPB20RHF80	14.706	17.067	6.457	12.385	0.148	0.171	0.957	2.113

the extent of WA, which can be evaluated using the following equation:

$$S = \frac{W_w}{W_c} \tag{5}$$

where W_w is the total mass of water absorbed in the equilibrium state and W_c is the initial mass of the composite sheet. Meanwhile the permeability is estimated by the product of the D and S.[10]

As can be seen in Table III, the M_m, D, S, and P all increase with the RHF loading for the biocomposites investigated in both the distilled and seawater condition. These findings are in agreement with previously reported work.[8,10,18] According Kwon et al.,[5] raw RHs comprise of 25%–35% cellulose, 18%–21% hemicellulose, 26%–31% lignin, 15%–17% silica, 2%–5% of soluble components, and 7.5% moisture. Most of the components have polar groups, that is, hydroxyl groups which tend to create hydrogen bonds with water (polar solvent). With the increasing fiber content, the adhesion between the fiber and matrix decreased because of the presence of the high void content and fiber–fiber interaction; hence, the M_m, D, S, and P values are higher.[43]

Interestingly, the difference in D between PB types and immersion environments, was more predominant in the biocomposites at higher levels of fiber loading (60 wt % and above). At 40 wt % fiber loading (higher content of polymer matrix) for MAPE coupled RHF composites, types of PB matrix (UPB/CPB) did not have a significant effect on the WA. At 80 wt % fiber loading (lower amount of polymer matrix), note that a remarkable decrease in M_m, D, S, and P values was observed for the biocomposites fabricated with CPB as compared with composites based on UPB. This was confirming the reduction in WA. The possible reason is the free hydroxyl and carboxyl groups available in hydrophilic rPET play the role of absorbing water if there are no chemical crosslink between polar rPET and nonpolar rHDPE chains with the aids of compatibilizer in the UPB matrix.[44] The immiscible rHDPE and rPET components in UPB tend to create small voids or microgaps between them, and thus enhancing the diffusion process. However, the presence of E-GMA compatibilizer tends to bind the rHDPE and rPET together and thus, reducing the hydrophilicity of CPB matrix as well as the WA.

In the case of the composites fabricated with UPB matrix, the D value was lower if the specimen was immersed in seawater compared with distilled water. This is because of the presence of large ionic salt molecules (notably sodium chloride) in the seawater which tends to slow the diffusion process of water molecules into the matrix.[20,37,42] In distilled water, pure water molecules are more easily diffusing through the pores between the immiscible rHDPE–rPET polymer chain. Interestingly, the biocomposites fabricated with CPB matrix exhibited a reverse trend, which is found to be more pronounced in seawater compared with distilled water. It is believed that salt in seawater somehow induces the formation of microcavities in the crosslink network of the CPB material.[45] This enhances the transportation of water molecules within the induced microcracks and thus increasing the WA and rate of moisture diffusion.

Modeling WA Behavior. In Fick's model, the WA increases linearly with the square root of time, and then gradually slows until a steady state, at which M_m is attained. The theoretical WA can be predicted using Fick's second law of diffusion.

For the initial portion of the curve where M_t/M_m is lower than 0.6,[41] it can be correlated using:

$$\frac{M_t}{M_m} = \frac{4}{h}\sqrt{\frac{D \cdot t}{\pi}} \tag{6}$$

For the second half-sorption curve where M_t/M_m is higher than 0.6,[41] an approximation is proposed by Shen and Springer as per the following equation:[46]

$$\frac{M_t}{M_m} = 1 - \exp\left[-7.3\left(\frac{D \cdot t}{h^2}\right)\right]^{0.75} \tag{7}$$

Figures 7 and 8 depict the long-term WA of RHF/PB biocomposites measured following immersion in distilled water and seawater, respectively. The solid curves show the prediction of theoretical WA behavior using Fick's second law of diffusion. The Fick's model curves were determined using eq. (6) for the linear portion and by using eq. (7) for the second portion. All the curves in both Figures 1 and 2 were found to follow Fickian type behavior, which conforms to the n coefficient (close to 0.5), calculated in Table II. Therefore, it can be generally concluded that the experimental results fit the Fickian mode of diffusion reasonably well, especially in the initial stage of diffusion. This result is consistent with previously reported work on natural fibers/polymer composites.[18,41]

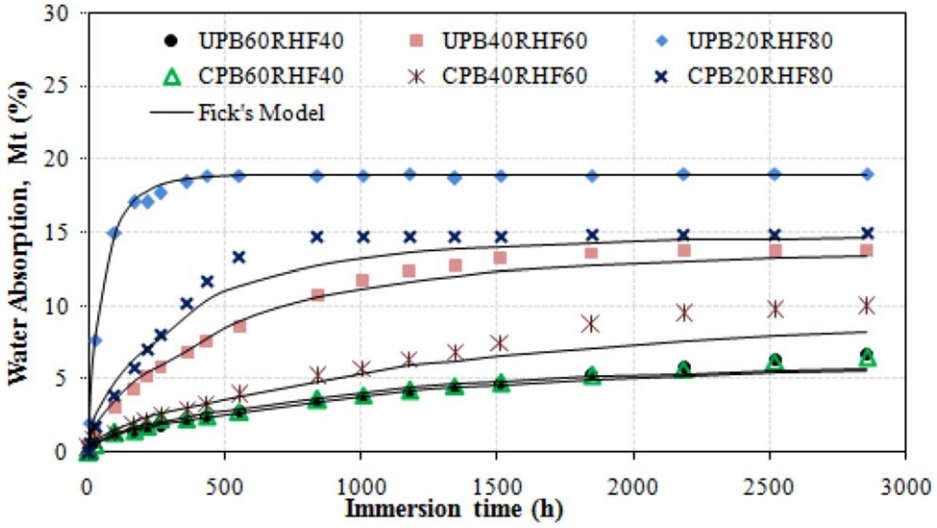

Figure 7. Water absorption of RHF biocomposites immersed in distilled water. [Color figure can be viewed in the online issue, which is available at wileyonlinelibrary.com.]

Modeling TS Behavior. The TS plays an important role in determining the stability performance of the composite, especially for those containing lignocellulosic fibers.[10] As known, lignocellulosic fibers possess the poor WA resistance which results in a moisture build-up in the fiber cell wall (fiber swelling) and in the fiber–matrix interface. This determines the dimensional changes of composites upon immersion in water. The swelling of the fiber induces stress and microcracks on the surrounding matrix, which leads to a weak fiber–matrix adhesion.[43] The swelling behavior in composites can be quantified by the model that proposed by Shi and Gardner,[47] which gives eq. (8) after being rearranged and taking the natural logarithm:

$$\ln\left(\frac{100\,T_\infty}{\mathrm{TS}(t)+100}-T_0\right)=\ln\left(T_\infty-T_0\right)-K_{\mathrm{SR}}t \qquad (8)$$

where TS(t) is the TS at time t; T_∞ and T_0 are the equilibrium and the initial thickness of specimen, respectively; and K_{SR} is the intrinsic relative swelling rate (a constant). The values of K_{SR} are dependent upon the swelling rate of the composite until the equilibrium TS is reached. A higher K_{SR} value means a higher swelling rate and thus the composite requires a shorter time to attain the equilibrium TS.[10,39] The results of TS measurement and the prediction of swelling rate parameter of biocomposites are presented in Table IV. The increase in RHF fiber content, irrespective of the types of PB matrix and immersion conditions, leads to an increase in the swelling rate. The trends of swelling rate as well as the relationship of types of matrix with immersion conditions are similar as the trends of WA.

For a comparison of how well the experimental data fits the model, the sum of squares is determined by eq. (9).

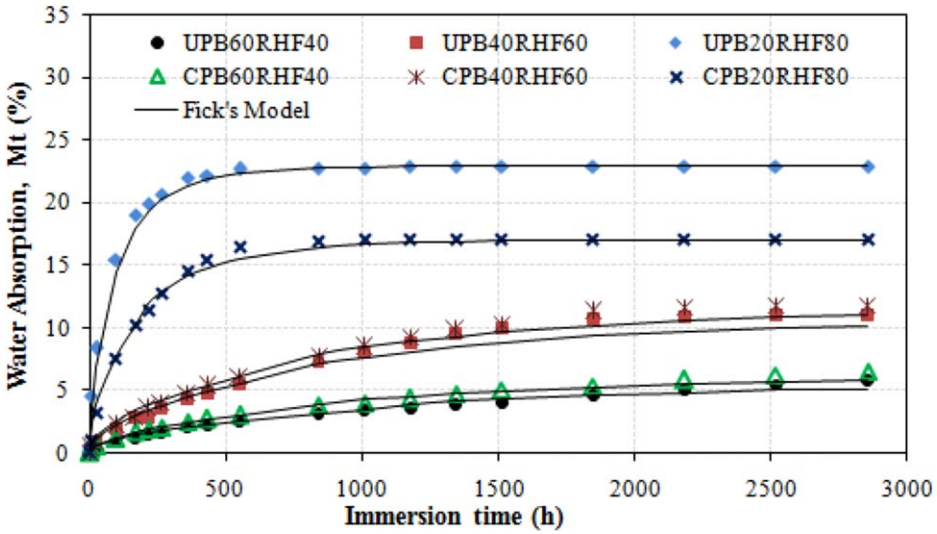

Figure 8. Water absorption of RHF biocomposites immersed in seawater. [Color figure can be viewed in the online issue, which is available at wileyonlinelibrary.com.]

Table IV. TS Measured and Swelling Rate Parameter Predicted for RHF/PB Biocomposites Under Distilled and Seawater Conditions

	T_O (mm)		T_∞ (mm)		TS_∞ (%)		$K_{SR} \times 10^{-3}$ (h^{-1})		SS	
Composite sample code	Distil	Sea	Distil	Sea	Distil	Sea	Distil	Sea	Distil	Sea
UPB60RHF40	3.00	2.94	3.09	3.04	2.78	3.75	3.321	1.852	0.723	1.278
UPB40RHF60	2.98	3.03	3.14	3.17	5.49	4.96	4.394	4.557	0.590	2.313
UPB20RHF80	3.44	3.47	3.63	3.63	5.42	6.45	22.694	8.522	2.970	6.254
CPB60RHF40	2.96	2.94	3.07	3.02	3.95	2.83	1.741	2.188	2.646	0.483
CPB40RHF60	3.36	3.33	3.53	3.48	4.56	4.82	2.212	5.626	2.773	1.407
CPB20RHF80	3.29	3.28	3.58	3.46	8.71	6.14	4.661	6.859	2.940	3.990

TS_∞, equilibrium thickness swelling.

$$SS = \sum_{i=1}^{n} (y_i - \hat{y})^2 \quad (9)$$

where n is the number of observations, and y_i and $\hat{y}$ are the observed and predicted values of the dependent variable, respectively. A better fit between the model and the experimental data is found for a lower SS value.[9,39]

The comparisons of the predicted TS from the swelling model [eq. (8)] and the measured experimental results are presented in Figure 9 for immersion in distilled water and in Figure 10 for immersion in seawater. Generally, the swelling model fitted better for the formulations immersed in distilled water (Figures 9 and 10) and their SS values were more consistent compared with those under seawater immersion (Table IV). From Table IV, it was also found that the SS value is proportional to the swelling rate (K_{SR}) and equilibrium TS (TS_∞).

As can be seen from Figures 9 and 10, a similar trend to the WA was observed, in which the swelling increased sharply in the initial stage for all fiber loadings, and then remained constant. The higher the fiber loading, the more hydrogen bonding was formed in the cell wall of lignocellulosic fiber by the adsorbed water, and therefore, the higher swelling of biocomposites was obtained.[43] Initially, the swelling of all UPB-based composites was greater than the CPB-based composites. This is possible due to the poor compatibility of PB matrix which may affect the dispersion and adhesion of RHF fiber in the composite, which allows the water to easily access into the cellulose.[10]

Comparison of WA and TS with Previous Studies. Table V describes the comparison of the D, M_m, K_{SR}, and TS_∞ with previously reported work on RH fiber/HDPE composite materials with different filler size and loading. Generally, a lower value of diffusion coefficients, swelling rate parameter, WA and TS at equilibrium state (M_m and TS_∞, respectively) were obtained from this study compared with previous studies. For example, the D and M_m of 80 wt % RHF–CPB composite calculated from this study are even lower than those RH–HDPE composites fabricated with only 60–65 wt % filler loading conducted by Najafi and Khademi-Eslam and Wang et al.[6,8] It is interesting to note that the calculated K_{SR} and TS_∞ from this study also have a lower value in comparison to those obtained by Najafi and Khademi-Eslam[6] for the same filler loading (60 wt %). This might indicate that the RHF/CPB composite considered in the

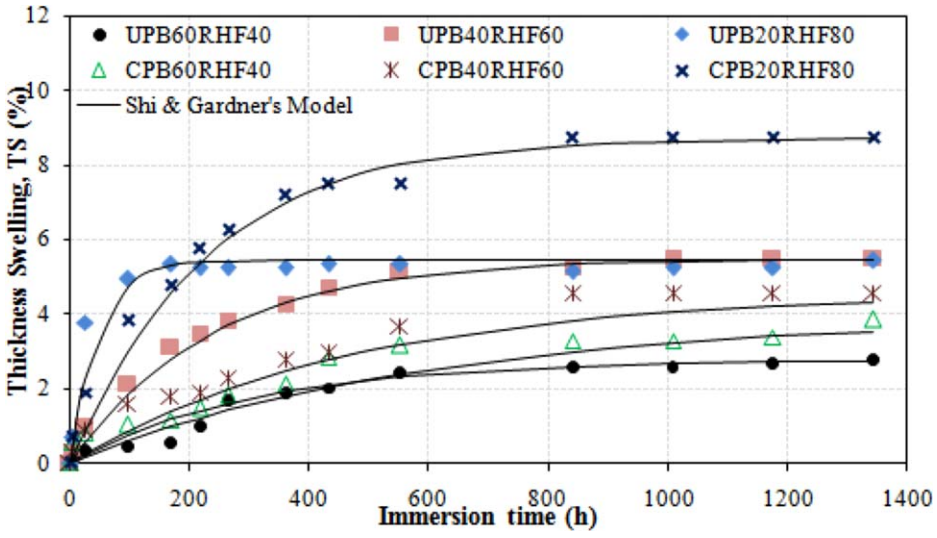

Figure 9. TS model fit for RHF biocomposites immersed in distilled water. [Color figure can be viewed in the online issue, which is available at wileyonlinelibrary.com.]

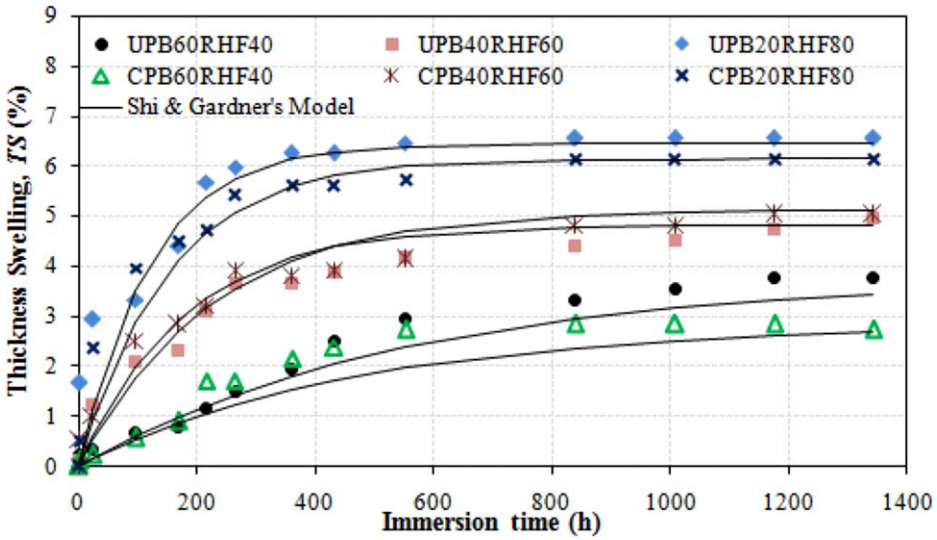

Figure 10. TS model fit for RHF biocomposites immersed in seawater. [Color figure can be viewed in the online issue, which is available at wileyonlinelibrary.com.]

current study has relatively better adhesion between the RH particles and PB matrix, and uniform dispersion of RHF throughout the matrix compared with other formulations.[21]

SEM

Figure 11 illustrates the morphology of the fracture surfaces of UPB, CPB, and their biocomposites incorporated with 40 and 80 wt % of RHF. Based on Figure 11(a,a′), the UPB displayed an incompatibility morphology of an obvious phase segregation structure between rHDPE and rPET, whereas the CPB exhibit a finer dispersion of rPET component inside the HDPE matrix. The presence of E-GMA as compatibilizer tends to improve the interfacial adhesion between the two phases, which resulted in an increment in mechanical properties.[48] The UPB-based biocomposites [Figures 11(b,c)] show a coarse morphology in the polymer matrices. From Figure 11(b), it can be clearly seen that the larger particle size shows no evidence of interfacial interaction and adhesion within the matrix phase, which confirms the incompatibility of the two matrix individual components.[49,50] Generally, we can see that the spherical rPET particles were not interacted with the rHDPE matrix as the holes and gaps has been seen at the interphase. Here, the black arrows in the Figure 11(b,c) show the available spaces or sites for the water molecules to diffuse and form hydrogen bonds with the polar rPET by breaking the existing bonds between the hydroxyl groups of the rPET chain.[51] Meanwhile, RHF reinforced composites with CPB matrices exhibited a finer surface morphology [Figure 11(b′,c′)] with smaller size matrix domains, which indicates the good dispersion or rPET particles inside the rHDPE matrix and the better interfacial adhesion within the matrix.[49] By comparing Figure 11(b/b′,c/c′), another striking observation can be seen. The RHF fillers at the concentration of 40 wt % were well

Table V. Comparison of D, M_m, K_{SR}, and TS_∞ with Previous Studies

Source	Polymer matrix	Filler/mesh size	Ratio matrix/filler/additive	$D \times 10^{-13}$ ($m^2\ s^{-1}$)	M_m (%)	$K_{SR} \times 10^{-3}$ (h^{-1})	TS_∞ (%)	Fabrication process
Current study	rHDPE/rPET/E-GMA (CPB)	RH/100	60/40/3	2.02	6.18	1.74	3.95	Corotating twin screw extruder/hot press
			40/60/3	1.63	9.96	2.21	4.56	
			20/80/3	6.46	14.71	4.66	8.71	
Najafi and Khademi-Eslam[6]	rHDPE	RH	40/60/3	51.40	25.0	2.90	6.18	Dry blend/hot press
Wang et al.[8]	vHDPE	RH/40	58/40/2	3.96	6.0	-	-	Hot press
			38/60/2	4.67	13.0			
			33/65/2	8.42	16.0			
Panthapulkkal et al.[40]	vHDPE	RH/30-60	35/65/2.5	-	9.28	-	6.30	Single screw extruder

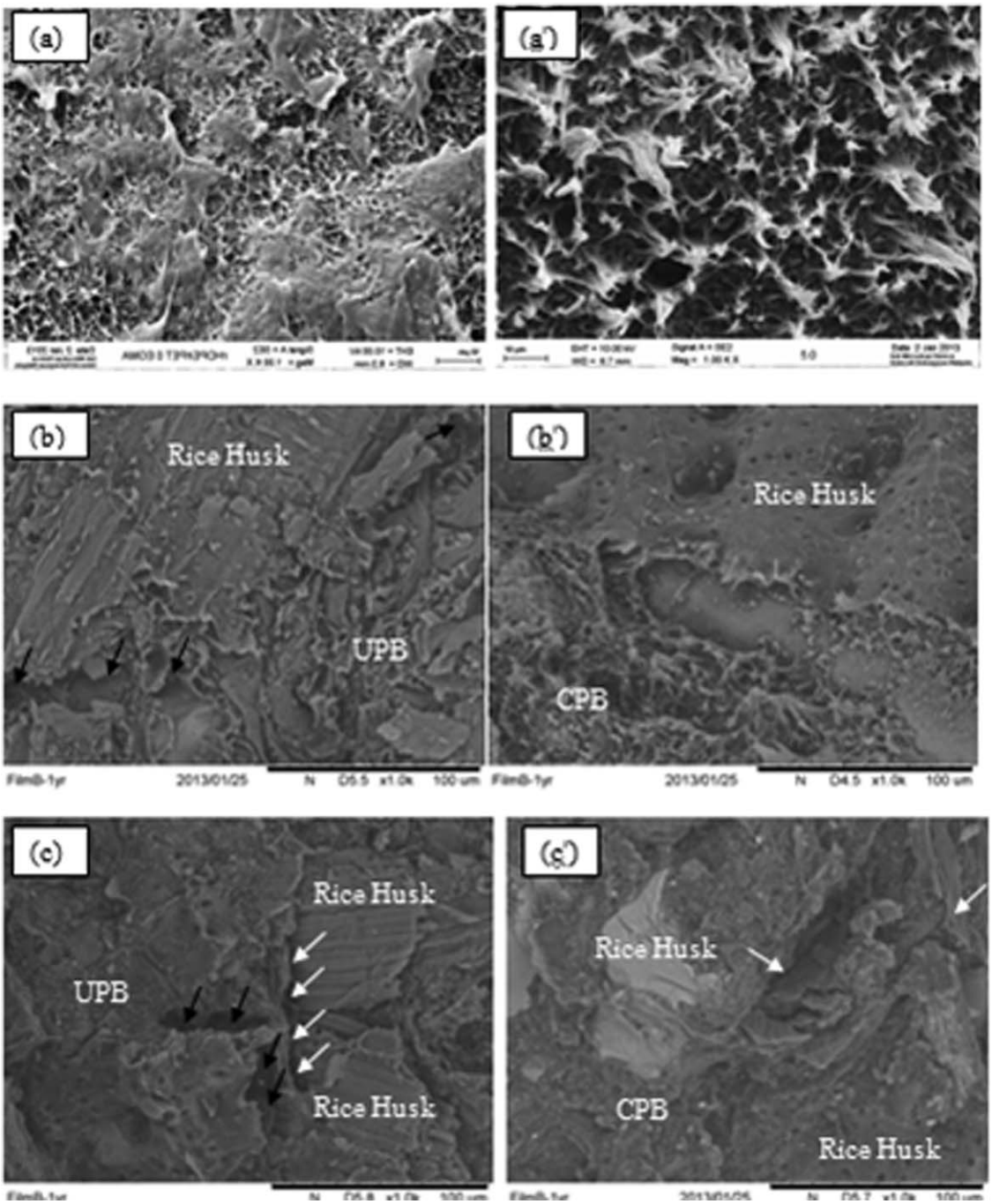

Figure 11. SEM micrograph of (a) 0 wt % UPB, (a′) 0 wt % CPB, (b) 40 wt % RHF–UPB composite, (b′) 40 wt % RHF–CPB composite, (c) 80 wt % RHF–UPB composite, and (c′) 80 wt % RHF–CPB composite, (magnification, 1000×).

embedded in the PB matrix. This phenomenon indicates the relatively good interface adhesion between the fibers and matrix. This accounts for the superior tensile and flexural modulus,[52] as supported by the results from Figures 2 and 5. Meanwhile, the white arrows in the latter figure show a clear gap between the polymer matrix and the RHF fillers which enhances the water diffusion. This was meant to indicate the poor filler–matrix interfacial bonding, as a result of insufficient amount of coupling agent at high RHF loading, that is, 80 wt %. Subsequently, the whole morphology of the composites has been affected by the uncompatibilized or compatibilized types of PB matrix as well as the filler loadings with the fixed amount of coupling agent.

CONCLUSIONS

RHF reinforced recycled HDPE/PET biocomposites have been fabricated by a two-step melt blending method. The types of PB

matrix (UPB and CPB) and agro-waste filler loadings has greatly influenced the morphology as well as WA and thickness stability. General, with increasing RHF content, the tensile and flexural properties of the biocomposites were significantly increased, especially the tensile and flexural modulus. In contrast, as expected, the addition of RHF into the PB matrices decreased the elongation to break and impact strength of the composites. However, the compatibilization of PB matrices by E-GMA compatibilizer increased the overall mechanical properties of CPB-based composites. In long-term water immersion test, the WA and TS increase with RHF content and immersion time for all types of biocomposite irrespective of the types of polymer matrix (uncompatibilized and compatibilized) and immersion condition (distilled and seawater). The diffusion coefficient, thermodynamic solubility and permeability obtained from the Fickian model, and the swelling rate parameter obtained from swelling model increased with the RHF content. However, all these parameters decreased with the compatibilization of PB matrix by E-GMA, especially at lower content matrix. Based on the results and findings in this work, it is proven that the agro-filler/recycled plastics composites are suitable for outdoor applications in terms of low WA and TS.

ACKNOWLEDGMENTS

The authors gratefully acknowledge The National University of Malaysia, BioComposites Extrusion Sdn Bhd, the Ministry of Higher Education Malaysia MyPHD Scholarship Programme and Technofund Grant TF0908D107 for the donation of materials and financial support.

REFERENCES

1. Kim, H.-S.; Lee, B.-J.; Choi, S.-W.; Kim, S.; Kim, H.-J. *Compos. Part A Appl.* **2007**, *38*, 1473.
2. Isa, K. M.; Daud, S.; Hamidin, N.; Ismail, K.; Saad, S. A.; Kasim, F. H. *Ind. Crops Prod.* **2011**, *33*, 481.
3. Chand, N.; Sharma, P.; Fahim, M. *Wear* **2010**, *269*, 847.
4. Zhao, Q.; Zhang, B.; Quan, H.; Yam, R. C. M.; Yuen, R. K. K.; Li, R. K. Y. *Compos. Sci. Technol.* **2009**, *69*, 2675.
5. Kwon, J. H.; Ayrilmis, N.; Han, T. H. *Compos. Part B Eng.* **2013**, *44*, 728.
6. Najafi, A.; Khademi-Eslam, H. *BioResources* **2011**, *6*, 2411.
7. Yang, H.-S.; Kim, H.-J.; Park, H.-J.; Lee, B.-J.; Hwang, T.-S. *Compos. Struct.* **2006**, *72*, 429.
8. Wang, W.; Sain, M.; Cooper, P. A. *Compos. Sci. Technol.* **2006**, *66*, 379.
9. Tajvidi, M.; Takemura, A. *J. Appl. Polym. Sci.* **2011**, *122*, 1258.
10. Adhikary, K. B.; Pang, S.; Staiger, M. P. *Chem. Eng. J.* **2008**, *142*, 190.
11. Lei, Y.; Wu, Q. *Bioresour. Technol.* **2010**, *101*, 3665.
12. Choudhury, A.; Kumar, S.; Adhikari, B. *J. Appl. Polym. Sci.* **2007**, *106*, 775.
13. Tarmudi, Z.; Abdullah, M. L.; Tap, A. O. *J. Teknol.* **2012**, *57*, 41.
14. Deka, B. K.; Maji, T. K. *Polym. Eng. Sci.* **2012**, *52*, 1516.
15. Fang, H.; Zhang, Y.; Deng, J.; Rodrigue, D. *J. Appl. Polym. Sci.* **2013**, *127*, 942.
16. Ashori, A.; Sheshmani, S. *Bioresour. Technol.* **2010**, *101*, 4717.
17. Alix, S.; Philippe, E.; Bessadok, A.; Lebrun, L.; Morvan, C.; Marais, S. *Bioresour. Technol.* **2009**, *100*, 4742.
18. Espert, A.; Vilaplana, F.; Karlsson, S. *Compos. Part A Appl.* **2004**, *35*, 1267.
19. Nourbakhsh, A.; Baghlani, F. F.; Ashori, A. *Ind. Crops Prod.* **2011**, *33*, 183.
20. Zamri, M. H.; Akil, H. M.; Bakar, A. A.; Ishak, Z. A. M.; Cheng, L. W. *J. Compos. Mater.* **2011**, *46*, 51.
21. Tamrakar, S.; Lopez-Anido, R. A. *Constr. Build. Mater.* **2011**, *25*, 3977.
22. Nosbi, N.; Akil, H. M.; Ishak, Z. A. M.; Bakar, A. A. *BioResources* **2011**, *6*, 950.
23. Mbarek, S.; Jaziri, M.; Chalamet, Y.; Carrot, C. *J. Appl. Polym. Sci.* **2010**, *117*, 1683.
24. Jayaraman, K.; Bhattacharyya, D. *Resour. Conserv. Recy.* **2004**, *41*, 307.
25. Chen, R. S.; Ab Ghani, M. H.; Ahmad, S.; Salleh, M. N.; Tarawneh, M. A. *J. Compos. Mater.* **2014**, 1.
26. Ab Ghani, M. H.; Salleh, M. N.; Chen, R. S.; Ahmad, S. *Am.-Eurasian J. Sustain. Agric.* **2014**, *8*, 128.
27. Nourbakhsh, A.; Ashori, A. *Bioresour. Technol.* **2010**, *101*, 2525.
28. Islam, M. N.; Rahman, M. R.; Haque, M. M.; Huque, M. M. *Compos. Part A Appl.* **2010**, *41*, 192.
29. Yao, F.; Wu, Q.; Liu, H.; Lei, Y.; Zhou, D. *J. Appl. Polym. Sci.* **2011**, *119*, 2214.
30. El-Shekeil, Y. A.; Sapuan, S. M.; Abdan, K.; S., Z. E. *Mater. Des.* **2012**, *40*, 299.
31. Ávila, A. F.; Duarte, M. V. *Polym. Degrad. Stab.* **2003**, *80*, 373.
32. Asgari, M.; Masoomi, M. *Compos. Part B Eng.* **2012**, *43*, 1164.
33. Hamid, M. R. Y.; Ab Ghani, M. H.; Ahmad, S. *Ind. Crops Prod.* **2012**, *40*, 96.
34. Yi, X.; Xu, L.; Wang, Y.-L.; Zhong, G.-J.; Ji, X.; Li, Z.-M. *Eur. Polym. J.* **2010**, *46*, 719.
35. Yang, H.-S.; Gardner, D. J.; Nader, J. W. *Compos. Part A Appl.* **2011**, *42*, 2028.
36. Adhikary, K. B.; Pang, S.; Staiger, M. P. *Compos. Part B Eng.* **2008**, *39*, 807.
37. Akil, H. M.; Cheng, L. W.; Ishak, Z. A. M.; Bakar, A. A.; Rahman, M. A. A. *Compos. Sci. Technol.* **2009**, *69*, 1942.
38. Abdul Khalil, H. P. S.; Nurul Fazita, M. R.; Jawaid, M.; Bhat, A. H.; Abdullah, C. K. *J. Compos. Mater.* **2011**, *45*, 219.
39. Osman, E. A.; Vakhguelt, A. *Int. J. Comput. Mater. Sci. Eng.* **2012**, *1*, 1.
40. Panthapulakkal, S.; Sain, M. *J. Compos. Mater.* **2007**, *41*, 1871.
41. Scida, D.; Assarar, M.; Poilâne, C.; Ayad, R. *Compos. Part B Eng.* **2013**, *48*, 51.

42. Nosbi, N.; Akil, H. M.; Mohd Ishak, Z. A.; Abu Bakar, A. *Mater. Des.* **2010**, *31*, 4960.
43. Shinoj, S.; Panigrahi, S.; Visvanathan, R. *J. Appl. Polym. Sci.* **2010**, *117*, 1064.
44. Ping, Z. H.; Nguyen, Q. T.; Chen, S. M.; Zhou, J. Q.; Ding, Y. D. *Polymer* **2001**, *42*, 8461.
45. Kahraman, R. *J. Appl. Polym. Sci.* **2005**, *98*, 1165.
46. Shen, C. H.; Springer, G. S. *J. Compos. Mater.* **1976**, *10*, 2.
47. Shi, S. Q.; Gardner, D. *J. Compos. Part A Appl.* **2006**, *37*, 1276.
48. Khan, Z. A.; Kamaruddin, S.; Siddiquee, A. N. *Mater. Des.* **2010**, *31*, 2925.
49. Lusinchi, J. M.; Boutevin, B.; Torres, N.; Robin, J. J. *J. Appl. Polym. Sci.* **2001**, *79*, 874.
50. El-Nashar, D. E.; Maziad, N. A.; Sadek, E. M. *J. Appl. Polym. Sci.* **2008**, *110*, 1929.
51. Célino, A.; Freour, S.; Jacquemin, F.; Casari, P. *Front. Chem.* **2014**, *1*, 1.
52. Singh, S.; Mohanty, A. K. *Compos. Sci. Technol.* **2007**, *67*, 1753.